1 **Bandgap engineering of polymetric carbon nitride copolymerized by**
2 **2,5,8-triamino-tri-s-triazine (melem) and barbituric acid for efficient nonsacrificial**
3 **photocatalytic H_2O_2 production**

4 Zhenyuan Teng[a,d,1], Wenan Cai[a,1], Sixiao Liu[c,d,1], Chengyin Wang[c,d,*], Qitao Zhang[b,*],
5 Chenliang Su[b], Teruhisa Ohno[a,d,*]

6

7 [a]*Department of Applied Chemistry, Faculty of Engineering, Kyushu Institute of*
8 *Technology, Kitakyushu 804-8550 Japan*
9 [b]*International Collaborative Laboratory of 2D Materials for Optoelectronics Science and*
10 *Technology of Ministry of Education, Institute of Microscale Optoelectronics, Shenzhen*
11 *University, Shenzhen, 518060, China*
12 [c]*College of Chemistry and Chemical Engineering, Jiangsu Key Laboratory of*
13 *Environmental Engineering and Monitoring, Yangzhou University, 180 Si-Wang-Ting*
14 *Road, Yangzhou 225002 China*
15 [d]*Joint Laboratory of Yangzhou University, Kyushu Institute of Technology, Yangzhou*
16 *University, 180 Si-Wang-Ting Road, Yangzhou 225002 China*
17 [1]*These authors contributed equally.*
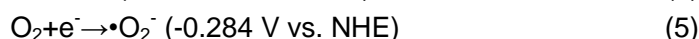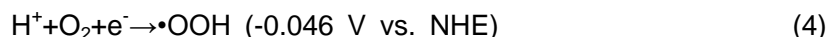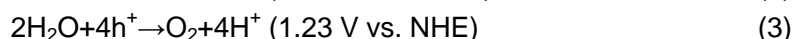
18

19 **Abstract**

20 Photocatalytic production of H_2O_2 from water and oxygen utilizing polymetric carbon

21 nitride (PCN) is a promising alternative to the energy-consuming anthraquinone method.

22 However, insufficient oxidation potential and limited light-absorption have restricted its

23 further improvement. Herein, PCN with sufficient oxidation potential and improved

24 visible-light usage (up to 550 nm) was prepared by co-polymerization of

25 2,5,8-triamino-tri-s-triazine (melem) and barbituric acid (BA). With the loading of

26 $Na_2CoP_2O_7$ as a water-oxidation co-catalyst, this novel PCN system showed a

27 record-high apparent quantum efficiency (420 nm) of 8.0% and a solar-to-chemical

28 conversion efficiency of 0.30% for H_2O_2 production. This improvement is attributed to the

29 introduced O 2p states by C=O groups remained in the PCN matrix, leading to a positive

30 valence band maximum of 1.85 eV (vs. SHE). The co-polymerization of BA and melem

31 combined with $Na_2CoP_2O_7$ loading also suppressed the charge recombination, resulting

32 in a rapid stepwise one-electron to one-electron reaction for efficient H_2O_2 production.

33

34 **Keywords:** Photocatalysis; nonsacrificial H_2O_2 production; band engineering; carbon

35 nitride; polymer design and synthesis;

36

1. Introduction

H$_2$O$_2$ is recognized as an industrially important green oxidant [1-4] and a promising future solar fuel (60wt% H$_2$O$_2$, 3.0 MJL^{-1}, higher energy density than that of compressed H$_2$ gas, 35 MPa, 2.8 MJL^{-1}) [5]. H$_2$O$_2$ is commonly generated by the reaction of anthraquinone with O$_2$. The as-obtained anthrahydroquinone was reduced to re-generate anthraquinone with H$_2$ on Pd-based catalysts [6]. As an alternative to this complicated energy-consuming process, direct synthesis of H$_2$O$_2$ with H$_2$ and O$_2$ has been achieved by utilizing Pd-based catalysts has been proposed [7,8]. By using this strategy, H$_2$O$_2$ is quantitatively generated, but the mixture of H$_2$/O$_2$ is naturally explosive. Processes for photocatalytic production of H$_2$O$_2$ on semiconductor materials have emerged as promising safe, environment-friendly, and energy-saving processes [9-19]. One of the most promising processes for photocatalytic H$_2$O$_2$ production is via water and O$_2$ (eq. 1) with an ideal atom efficiency up to 100% [15-18]. Both reduction of O$_2$ (eq. 2) via two electron transfer pathways and efficient water oxidation (eq. 3) are required for the photocatalyst to achieve this process.

$$2H_2O+O_2 \rightarrow 2H_2O_2 \tag{1}$$
$$O_2+2H^++2e^- \rightarrow H_2O_2 \ (0.695 \ \text{V vs. NHE}) \tag{2}$$
$$2H_2O+4h^+ \rightarrow O_2+4H^+ \ (1.23 \ \text{V vs. NHE}) \tag{3}$$
$$H^++O_2+e^- \rightarrow \bullet OOH \ (-0.046 \ \text{V vs. NHE}) \tag{4}$$
$$O_2+e^- \rightarrow \bullet O_2^- \ (-0.284 \ \text{V vs. NHE}) \tag{5}$$

Metal oxides and polymeric carbon nitrides (PCNs) based semiconductors have been widely studied for achieving photocatalytic H$_2$O$_2$ production since the band structures of metal oxides and PCNs are capable of catalyzing both of the reactions shown in eq. 2 and eq. 3. However, the selectivity of metal oxides for photocatalytic H$_2$O$_2$ production is quite low because 1-electron reduction of O$_2$ (superoxide (hydrogen peroxide radical formation (•OOH), eq. 4; •O$_2^-$) radical formation, eq 5) usually dominates, thus suppressing 2-electron reduction [20-25]. PCNs, which has been recognized as a promising metal-free photocatalyst under visible-light irradiation [26-27], can promote selective photoreduction of O$_2$ and produces H$_2$O$_2$ via the formation of 1-4 endoperoxide on 2,5,8-triamino-tri-s-triazine (melem) units by a rapid stepwise reaction via 1-e$^-$ pathway [16-18]. However, most of the PCN-based materials produce a large amount of H$_2$O$_2$ only

1 with the existence of electron donors [11-14, 19] since it seems that the holes captured in

2 the valence band maximum (VBM) of PCN (around 1.4~1.6 V vs. standard hydrogen

3 electrode, SHE) seems not positive enough to overcome the large potential for water

4 oxidation (c.a. > 0.8 V). To overcome this obstacle, Shiraishi and co-workers proved that

5 the co-polymerization of light adsorption units with C=O could significantly shift the band

6 position of PCN to the positive side, leading to an enhanced photocatalytic activity for

7 oxygen evolution reaction (OER) [15-17]. However, the reason of the band shift was not

8 clarified at the electronic energy level, and the large bandgap width of PCN (~2.7 eV),

9 even with co-polymerization of BDI [15, 17] or PDI [16], limits the ratio of the visible light

10 that can be used, resulting in limited solar to chemical conversion (SCC) efficiency (~

11 0.2%) [18].

12   Co-polymerization of barbituric acid (BA), which also contains a large amount of C=O

13 groups, has been used for narrowing the bandgap of PCN, a process that was firstly

14 reported by Zhang et al. [27-30]. The light adsorption range of PCN samples obtained by

15 co-polymerization of nitrogen-rich precursors and BA was significantly expanded [27-30].

16 However, the conduction band minimum (CBM) and VBM shift to the opposite side,

17 leading to suppressed photo-redox activity [27]. One possibility is that in the previously

18 reported mechanisms, BA molecules are directly incorporated into the classical carbon

19 nitride condensation scheme via an S_N2 nucleophilic substitution reaction (Scheme 1A)

20 [27]. In that scheme, the quaternary carbon atoms of BA molecules were nucleophilically

21 attacked by the amino groups of dicyandiamide, and then the oxygen groups are

22 removed from the PCN matrix [27]. To keep the C=O groups in the PCN matrix, the S_N2

23 nucleophilic substitution has to be suppressed during the co-polymerization. Typically,

24 this nucleophilic addition would be suppressed if the molecular weights of nucleophilic

25 regents are increased, i. e., the steric hindrance effect could be improved (Scheme 1B).

26 As a result, the deamination selectivity could be enhanced. Thus, C=O groups could

27 remain during the thermal polymerization if precursors with large molecular weights are

28 used. Melem (Scheme 1C), as an intermediate product during the thermal polymerization

29 of PCN with a large molecule weight [32], could serve as an ideal co-polymerization

3

precursor for co-polymerization with BA. The molecular weight of melem (218.1) is more than 2-times larger than that of dicyandiamide (84.1), leading to a large steric effect that can suppress the S_N2 nucleophilic substitution. Therefore, co-polymerization of melem and BA (Scheme 1C) enabled the introduction of C=O groups into the PCN matrix, leading to an improved photocatalytic water oxidation activity with promoted light usage of the PCN-based photocatalyst.

Here is Scheme 1.

Herein, we engineered the band positions of polymetric carbon nitride prepared by using barbituric acid and melem as precursors (denoted as PCNBA). The C=O groups were maintained in the as-prepared PCN matrix, and the band positions of the as-prepared PCNBA shifted positively with a sufficient oxidation potential (up to 1.85 V vs. SHE) for water oxidation. The narrowed bandgap width ranging from 2.77 eV to 2.18 eV also significantly expanded the adsorption range of solar light. Furthermore, the reason of the band shift caused by the co-polymerization of barbituric acid was clarified at the electronic level by combining the results of XPS measurements and density functional theory (DFT) simulations. With the optimized co-polymerization and loading of $Na_2CoP_2O_7$ as an OER co-catalyst [33], the PCNBAs showed a high apparent quantum yield (ΦAQY) of 8.0% and SCC efficiency of 0.30% for photocatalytic H_2O_2 production with only H_2O and O_2. Moreover, the co-relationships between the charge separation and the photocatalytic activities for H_2O_2 production were clarified for the first time. This work provides a primary guideline and a practical approach for designing materials with an appropriate band structure to achieve optimized performance for photocatalytic H_2O_2 production.

2. Experimental details
2.1 Preparation of photocatalyst

Unless otherwise stated, the purities of all reagents for preparation of photocatalysts preparation and for photoelectrochemical measurements were above analytical grade. Melem was prepared by calcination of melamine at 420 °C in N_2 for 4 h. [32] The polymetric carbon nitride with barbituric acid co-polymerization (PCNBA) was prepared as follows: 3 g melem with a certain amount of barbituric acid (SIGMA-ALDRICH, Co.,

1 Ltd.) was ball-milled in the presence of ethanol for 2 h (400 rpm). Then the mixture was

2 drying in a vacuum oven at 60 °C for 4 h. The as-obtained white powder was calcinated in

3 a furnace at 560 °C in air for 4h with an increasing temperature rate of 2 °C. The bulk

4 material was obtained when the furnace was cooled down to room temperature. The

5 adding amounts of barbituric acid (BA) added were 0.01 g, 0.05 g, 0.1 g, 0.2 g and 0.5 g.

6 These samples were named PCNBA0.01, PCNBA0.05, PCNBA0.1, PCNBA0.2 and

7 PCNBA0.5, respectively.

8 $Na_2CoP_2O_7$ was prepared by following previous reports. Na_2CO_3 (1. 06 g, Wako

9 Pure Chemical Industries, Ltd.), $CoNO_3 \cdot 6H_2O$ (2.91 g, Wako Pure Chemical Industries,

10 Ltd.) and $(NH_4)_2HPO_4$ (2.64 g, Wako Pure Chemical Industries, Ltd.) were ball-milled with

11 acetone for 1 h. Then the purple mixture was dried in a vacuum oven for 8 h at 25 °C. The

12 purple powder was calcined at 600 °C for 16 h. After cooling down to the room

13 temperature, blue bulk material was obtained [34].

14 The loading of $Na_2CoP_2O_7$ onto the PCNBA was conducted using a simple ball

15 milling method. Specifically, the 0.2 g of PCNBA samples with a certain amount of

16 $Na_2CoP_2O_7$ (0.002 g, 0.005 g, 0.01 g and 0.02 g) was ball-milled for 15 min. The

17 as-prepared samples were named PCNBAxCo1%, PCNBAxCo2.5%, PCNBAxCo5% and

18 PCNBAxCo10%, respectively.

19

20 **2.2 Measurements of photocatalytic activities**

21 Each catalyst (50 mg) was added to pure water (30 mL) within a borosilicate glass

22 bottle (φ 45 mm; capacity, 50 mL), and the bottle was sealed with a rubber septum cap.

23 The catalyst was dispersed well by ultrasonication for 15 min, and O_2 was bubbled

24 through the solution for 30 min. The bottle was immersed in a temperature-controlled air

25 bath at 298 ± 0.5 K with wind flowing and was photo-irradiated at λ > 420 nm using a 500

26 W Xe lamp (PXE-500, USHIO Inc.) with magnetic stirring. Water oxidation with $AgNO_3$ as

27 a sacrificial electron acceptor was performed with a catalyst (100 mg) in a buffered La_2O_3

28 (30 mg) solution (30 mL, pH 8−9) with $AgNO_3$ (10 mM) under an Ar atmosphere (1 atm).

29 The amount of H_2O_2 was determined by a colorimetric method using PACKTEST (WAK-

30 H_2O_2, KYORITSU CHEMICAL-CHECK Lab., Corp.) equipped with a digital PACKTEST

5

1 spectrometer (ED723, GL Sciences Inc.).

2

3 **2.3 Action spectrum analysis.**

4 Photocatalytic reactions were carried out in pure water (30 mL) with catalysts (50 mg)

5 with or without the addition of et-OH as an electron donor reagent. After ultrasonication

6 and O_2 bubbling, the bottle was photoirradiated photoirradiated by a Xeon lamp for 6 h

7 with magnetic stirring. The incident light was monochromated by band-pass glass filters

8 (Asahi Techno Glass Co.), where the full-width at half-maximum of the lights was 11−16

9 nm. The numbers of photons that entered into the reaction vessel was determined with a

10 3684 optical power meter (HIOKI E.E. CORPORATION).

11

12 **2.4 Determination of SCC efficiency.**

13 Solar to chemical conversion (SCC) efficiency was determined by photoreactions

14 with a PEC-L01 solar simulator (Peccell Technologies, Inc.). Photoreactions were

15 performed in pure water (100 mL) with catalysts (each 500 mg) under O_2 (1 atm) in a

16 borosilicate glass bottle, with λ > 420 nm cutoff filter was used to avoid subsequent

17 decomposition of the formed H_2O_2 by absorbing UV light [18]. The irradiance of the solar

18 simulator was adjusted to the AM1.5 global spectrum.[15] The SCC efficiency was

19 calculated by the following equation:

20 $$SCC(\%) = \frac{\Delta G_{H_2O_2} \times n_{H_2O_2}}{t_{ir} \times S_{ir} \times I_{AM}} \times 100\%.$$

21

22 In the equation, $\Delta G_{H_2O_2}$ is the free energy for H_2O_2 generation (117 kJ mol^{-1}). $n_{H_2O_2}$

23 is the amount of H_2O_2 generated, and t_{ir} is the irradiation time (s). The overall irradiation

24 intensity (I_{AM}) of the AM1.5 global spectrum (300−2500 nm) is 1000 W m^{-2}, and the

25 irradiation area (S_{ir}) is 0.628 × 10^{-4} m^2 [15].

26 Detailed information on **Instruments**, **Radiative oxygen species measurements**,

27 **Photoelectrochemical characterizations** and **Calculation details** is shown in the

28 *Supporting information*.

29

30 **3. Results and discussion**

31 **3.1 Characterization of PCNBA**

1   Successful synthesis of PCNBA from melem with copolymerization of barbituric acid

2   was confirmed by XRD, TEM, SAED, EDS-mapping, and FT-IR absorption and XPS

3   spectral analyses (Figure 1). XRD measurements were first used to investigate the

4   crystallinity changes after co-polymerization of PCN when the amount of BA added was

5   increased from 0.01 g to 0.5 g (Figure 1A). The two characterization diffraction peaks at

6   13.1° and 27.4° did not show any obvious shift, indicating that the interplanar spacing did

7   not change [27, 31]. Additionally, the peaks at 13.0° assigned to the c-axis remained

8   almost constant, whereas the intensity of the interlayer (002) peak at 27.4° clearly

9   decreased. These results might be due to the disturbance of the graphitic structure by

10   inserting BA motifs in the layered structure. Selected area electronic diffraction patterns

11   of PCNBA (inserted in Fig. 1B) also revealed that the crystalline structure of PCN did not

12   change after the addition of the motifs. Therefore, the crystalline structure of the PCN

13   matrix after BA co-polymerization almost remained constant compared with the pristine

14   ones [35].

15   **Here is Figure 1.**

16   To investigate the elemental distribution differences between pristine PCN and

17   PCNBA, scanning TEM-energy-dispersive X-ray spectroscopy (STEM-EDS) mappings

18   were conducted. PCNBA0.2 was selected as a representative example of all PCNBA

19   samples due to its optimum motif addition concentration. As shown in Figure S1-2 and

20   Figure 1B, the morphologies of pristine PCN and PCNBA0.2 are quite similar, whereas

21   the oxygen content of PCNBA0.2 is slightly increased (Figures 1C). It was also found that

22   after copolymerization with BA, the oxygen homogenously distributed in the PCN matrix.

23   To further investigate the functional groups of PCNBA0.2 after co-polymerization, Fourier

24   transform infrared (FT-IR) spectroscopy was performed. The FTIR spectra (Figure 1D)

25   exhibited all of the characteristic stretch modes of aromatic CN heterocycles and the

26   breathing mode of heptazine units at 1200-1700 cm^{-1} and 700-900 cm^{-1}, respectively [31,

27   35]. Additionally, the broad peaks between 2900 cm^{-1} and 3500 cm^{-1} could be assigned to

28   hydroxyl (-OH) stretching (the adsorption water) and N-H stretching (PCNBA skeleton),

29   indicating that the NH and/or NH_2 groups exist in the PCN matrix [31, 35]. Although

30   PCNBA0.2 showed fundamental groups similar to those of the pristine PCN, the oxygen

1   groups could hardly be identified by FTIR since due to overlap of heptazine breathing

2   (1200-1700 cm^{-1}) and carbonyl stretching (1700 cm^{-1}) [35, 36].

3   To further investigate the chemical composition and chemical states in as-prepared

4   samples, XPS measurements were conducted. The survey spectra of pristine PCN

5   revealed that only C and N elements exist (Figure S3), with a very small amount of O

6   element that was due to the H_2O adsorption (Figure S5A, 532.5 eV). In the case of

7   PCNBA, the O 1s peak gradually increased with the increasing addition of BA motifs, and

8   a newly deconvoluted peak at 531.8 eV could be assigned to the existence of C=O

9   groups in the PCN matrix (Figure S3 and S5B-5D) [35]. In the case of the C 1s

10 high-resolution XPS spectra (Figure S4), the peak at 287.9 eV was assigned to N-C-N

11 coordination, and the other deconvoluted peak at 284.6 eV was due to sp^2 C-C bonds

12 resulting from the carbon-adsorption contamination [31, 35, 37]. When BA was used in

13 the co-polymerization, there was a newly deconvoluted peak at 288.7 eV that was

14 assigned to the C=O coordination, which supports the results of O 1s spectra. In the

15 high-resolution XPS spectrum of N 1s (Figure 1E), the three deconvoluted peaks

16 observed at 401.1 eV, 400.1 eV and 398.8 eV were assigned to amino groups C-N-H,

17 tertiary nitrogen groups, and sp^2 C-N-C bonds, respectively [35, 37]. Furthermore, the

18 greater number of the BA units used in the co-polymerization was, the higher was the

19 intensity of the peak at 400.1 eV. This result can be attributed to the co-polymerization

20 nature of melem and BA (Figure 1F). When BA units were inserted into the melon

21 molecules, the number of tertiary nitrogen groups of PCN-BA would increase accordingly.

22 Further evidence is that the intensities of deconvoluted peaks at 284.6 eV (C-C) and

23 533.1 eV (O=C) gradually increased when the concentration of motifs (BA units)

24 increased, indicating the existence of BA in the PCN matrix. Therefore, these results

25 collectively indicated the well-preserved structure of PCN as well as the successful

26 construction of BA units with the existence of C=O-based covalent networks through this

27 copolymerization synthesis.

28   **Here is Figure 2.**

29   The morphologies of bare PCN and PCNBA were investigated by TEM and BET

30 measurements. As shown in Figure S1 and Figure 1B, both pristine PCN and PCNBA0.2

showed a bulky morphology. As shown in Figure S6A, the surface area of PCNBA0.2 (2 m^2g^{-1}) was only slightly smaller than that of pristine PCN (3 m^2g^{-1}), which was also supported that the bulk morphology of the PCNBA0.2. The pore size and pore volume of the PCNBA0.2 decreased slightly when BA units were introduced to the PCN matrix. Since the holes formed in bulk PCN material are attributed to the secondary particle piled pores, the slight decrease of PCNBA0.2 may be attributed the smaller particle size of PCNBA0.2 compared with that of pristine PCN. As shown in Figure S7, PCNBA prepared with BA and melem showed a macroscopic deep orange color, rather than the pale yellow of pristine PCN, providing the success in the improved visible-light absorption [31, 35]. To determine the precise band positions of PCNBAs, UV-vis, Mott-Schottky measurements and valence band XPS were conducted to investigate the bandgap width, CBM and VBM, respectively. As shown in Figure 2A, the light adsorption (<450 nm) of PCNBAs significantly increased, possibly due to the changes in electronic states [13]. With increased addition of BA motifs, the adsorption of long-wave visible light gradually increased, resulting in the narrowing of bandgap width from 2.77 eV to 2.18 eV. Mott-Schottky plots revealed that the CBM of PCNBA samples gradually became more positive from -1.33 eV for pristine PCN to -0.33 eV for PCNBA0.5 (Figure S8). VB-XPS results also showed that the VBM of PCNBA gradually became positive from 1.45 eV to 1.85 eV (Figure 2B). By summarizing these results for band positions, we can draw band position diagrams of pristine PCN and PCNBA samples, as shown in Figure 2C. Generally, an ideal photocatalyst for H_2O_2 production from dissolved O_2 and water usually has two crucial properties: one is reducing O_2 to effectively produce H_2O_2 (eq. 2) and the other is sufficient oxidization potential for overcoming the large overpotential of water oxidation (eq. 3). Since the melem units in the PCN matrix can form 1,4-endoperoxides for efficient H_2O_2 production, the bottleneck of improving photocatalytic H_2O_2 production by PCN from water and O_2 is to overcome the insufficient oxidation potential (VBM_{PCN}=1.45 eV vs. a standard hydrogen electrode, SHE) for water oxidation. Compared with other samples, PCNBA0.1, PCNBA0.2 and PCNBA 0.5 eV all had positive VBMs at 1.85 eV (vs. SHE), indicating that water oxidation might occur on these

1   catalysts, thus leading to an effective H_2O_2 production from O_2 and water.

2   **Here is Figure 3.**

3   To further improve the overall H_2O_2 production by PCNBA from water and O_2, loading

4   a co-catalyst for water oxidation is an effective strategy since the VBM of PCNBA is still

5   more negative than those of traditional photocatalysts for water oxidation such as TiO_2

6   [38], Ta_2O_5 [39], WO_3 [40, 41], $BiVO_4$ [42]. Therefore, $Na_2CoP_2O_7$, one of the most

7   efficient co-catalysts for water oxidation, was prepared for enhancing the water oxidation

8   [33]. X-ray diffraction (XRD) patterns of the synthesized $Na_2CoP_2O_7$ matched excellently

9   with those in previous reports without impurities [33, 34, 44]. After loading $Na_2CoP_2O_7$ on

10 PCNBA0.2 by a facile ball milling method, the characterization peak of PCN at diffraction

11 angles of 13.1° and 27.4° still existed, indicating that the crystalline structure was well

12 maintained. Additionally, the peak intensities of $Na_2CoP_2O_7$ diffractions gradually

13 increased with an increase in the loading amount, indicating that $Na_2CoP_2O_7$ also

14 maintained the same structure after the ball milling. To investigate the distribution

15 properties of $Na_2CoP_2O_7$, high-angle annular dark field (HAADF) STEM combined with

16 energy-dispersive X-ray spectroscopy (STEM-EDS) mappings were conducted. As

17 shown in Figure 3C, some bright particles were dispersed well on the large bulk material,

18 and the average particle size was ~20 nm. EDS mapping showed that the elemental

19 components of the large bulk material contain high concentrations of carbon, nitrogen

20 and oxygen, which is consistent with the mapping image of PCNBA0.2. As shown in

21 Figure 3G-I, the elemental compositions of bright particles in Figure 3C are Na, P and Co,

22 indicating that these particles are $Na_2CoP_2O_7$. Therefore, the proposed ball milling

23 strategy could effectively disperse $Na_2CoP_2O_7$ onto PCNBA samples. The surface area of

24 PCNBA0.2Co5% (2 m^2g^{-1}) is almost as same as that of pristine PCNBA0.2 (2 m^2g^{-1}),

25 indicating that loading of the co-catalyst did not significantly change the morphology of

26 PCNBA0.2 (Figure S6A, Figure 3C). Additionally, pore size and pore volume were further

27 decreased after the co-catalyst loading, indicating that the loaded $Na_2CoP_2O_7$ particle

28 has filled pores piled by secondary particles (Figure S6B). The BET analysis further

29 supported the TEM and STEM-EDS mapping results, demonstrating the successful

30 loading of co-catalyst. UV-vis was conducted to determine the effect of $Na_2CoP_2O_7$

1   loading on the light absorption properties of PCNBA since $Na_2CoP_2O_7$ could naturally

2   absorb orange light (Figure 3J, blue line.). The UV-vis spectrum of PCNBA loaded with

3     $Na_2CoP_2O_7$ (mass ratio of 5%) is almost as same as that of PCNBA0.2 except for a small

4   absorption band that appeared between 550 nm and 650 nm. This small adsorption band

5   may be due to the light absorption introduced by $Na_2CoP_2O_7$. Tauc-plots (Figure S9),

6   Mott-Schottky plots (Figure S10) and VB-XPS measurements (Figure S11) also

7   confirmed that the band positions did not change after $Na_2CoP_2O_7$ loading. Therefore,

8   uniformly dispersed $Na_2CoP_2O_7$ particles on PCNBA0.2 could serve as a co-catalyst to

9   further improve the photocatalytic water oxidation, leading to an improved H_2O_2

10   production.

11

12 **3.2. Photocatalytic activities of PCNBA and PCNBACo for H_2O_2 production**
13   **Here is Figure 4.**

14   Since the inefficient water oxidation of PCN (VBM ranging from 1.4 eV-1.6 eV vs.

15   SHE), most of photocatalytic production of H_2O_2 based on PCN system were investigated

16   by utilizing electron donors. The band position of PCNBA samples is positively shifted

17   (Figure 3K), i.e., the photocatalytic water oxidation ability should be improved. Therefore,

18   the condition of photocatalytic H_2O_2 production must be investigated with and without the

19   addition of electron donors (ethanol). First, the optimized BA unit concentration was

20   investigated, as shown in Figure 4A. The activity of pure PCN for H_2O_2 production is quite

21   low, whereas the PCN samples with BA motifs all exhibited markedly increased activities.

22   Among the various PCN samples modified with BA, the activity of PCNBA0.2 was the

23   highest which is the 9.6-fold compared with that of PCN counterpart. It should be noted

24   that PCNBA0.5 produced less than half the amount H_2O_2 compared with PCNBA0.2,

25   which may be attributed to the positive shift of CBM (-0.33 V vs. SHE). Since O_2 reduction

26   to generate H_2O_2 is a multi-electron transfer reaction, the overpotentials of multi-electron

27   transfer reactions are non-negligible. For instance, hydrogen evolution reactions usually

28   need >0.4 V without loading Ni or Pt as HER cocatalysts. The relatively positive CBM of

29   PCNBA0.5 may not provide sufficient potentials for efficient O_2 reduction via two-electron

30   pathways.

1   The optimal pH conditions were investigated by measuring photocatalytic H_2O_2

2   production by utilizing PCNBA0.2 (Figure S12). When ethanol was introduced into the

3   system, the amount of H_2O_2 remained almost constant when the pH value was increased

4   from 1 to 9 and then decreased drastically. This result indicates that the lowest $[H^+]$ is 10^{-9}

5   mol/L for the O_2 reduction to H_2O_2 production. When no sacrificial agent was added into

6   the system, the amount of H_2O_2 rapidly increased before the pH value reaches 7 and

7   then gradually decreased, indicating that a low concentration of OH^- also restricts the

8   generation of O_2 from water [11, 44]. Therefore, the optimal pH condition for H_2O_2

9   production from O_2 and water is 7-9. The optimal solution was also investigated, as

10   shown in Figure S13. A photocatalyst in phosphate buffer solution (PBS) showed the

11   highest activity for H_2O_2 production with or without the existence of ethanol. This is

12   thought to be because phosphate ions can serve as a stabilizer for H_2O_2 under light

13   irradiation [11]. The pH value of the phosphate buffer ranges from 5.5 to 8.5, which is also

14   consistent with the optimal pH condition for H_2O_2 production. Figure 4B shows the

15   time-dependent change of the amounts of H_2O_2 produced. The generation rates of H_2O_2

16   on PCNBA0.2 and PCNBA0.2Co5% kept almost constant even after long-term reaction,

17   indicating that the catalyst could continuously produces H_2O_2 with good stability. Figure

18   4C shows the action spectrum on PCNBA0.2 and PCNBA0.2Co5% determined by light

19   irradiation for H_2O_2 production. Compared with the absorption spectra of the catalyst, the

20   ΦAQYs agree well, which shows that the production of H_2O_2 is attributed to the bandgap

21   excitation of PCNBA0.2. ΦAQYs at 420 nm of PCNBA0.2 and PCNBA0.2Co5% were

22   determined to be 4.0% and 8.0%, respectively, much which are higher than that (6.1%) of

23   g-C_3N_4/PDI/rGO0.05 [15], one of the most efficient PCN-based photocatalysts for

24   nonsacrificial H_2O_2 production. Additionally, the action adsorption edge extend form 450

25   nm for g-C_3N_4/PDI/rGO0.05 to 550 nm for PCNBA0.2 and PCNBA0.2Co5%, indicating

26   that the band engineering with BA units significantly promoted the photon usage. The

27   ΦAQY of PCNBA0.2Co5% was almost two-times larger than that of PCNBA0.2, and no

28   H_2O_2 was produced by the excitation between 550 nm and 650 nm, indicating that the

29   excitation introduced by $Na_2CoP_2O_7$ does not produce H_2O_2, i. e. $Na_2CoP_2O_7$ plays a role

12

1 as a co-catalyst during photocatalytic H_2O_2 production. The SCC efficiency for H_2O_2

2 production on PCNBA0.2Co5% was measured by AM1.5G solar simulator (1 sun

3 irradiation) to be 0.30% (see Experimental Section) and was almost constant even after

4 the photoirradiation for 2 h. As shown in Figure S14, the adsorption band at 600-900 cm^{-1}

5 and 1200-1700 cm^{-1} scarcely changed after the 5 run, indicating the functional groups of

6 PCNBA0.2 kept almost constant after the reaction. The XRD of the samples obtained

7 after 5 circles showed similar diffraction patterns as the raw sample, indicating that the

8 crystallinity of PCNBA0.2 and $Na_2CoP_2O_7$ rarely changed during the photocatalytic H_2O_2

9 production. The intensities of the diffractions contributed by $Na_2CoP_2O_7$ showed a slight

10 decrease. This slight decrease may be due to the loaded co-catalyst slightly detached

11 during the long-time stirring during the H_2O_2 production. After 5 cycles of measurements,

12 the efficiency was still maintained at 90% (Figure S15), indicating the good stability of the

13 catalyst. The SCC efficiency of PCNBA0.2Co5% is comparable to the highest levels

14 obtained by PCN-based photocatalysts (Figure 4D), suggesting that band engineering

15 combined with co-catalyst loading has great potential for the development of highly

16 efficient photocatalysts with improved activity for nonsacrifical H_2O_2 production. This

17 strategy would also inspire other artificial photosynthesis, such as overall water splitting,

18 N_2 fixation, etc. [15-18, 45].

19

20 **3.3 Mechanism of photocatalytic H_2O_2 production**
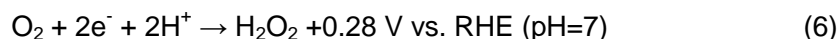
21   **Here is Figure 5.**

22   As shown in the photoluminescence (PL) spectra (Figure 5A), there was a redshift

23 toward a longer wavelength with an increase in the modified content of BA together with a

24 notable decrease in intensity, being consistent with previous reports [31, 35]. Additionally,

25 loading of $Na_2CoP_2O_7$ did not change the emission wavelength, whereas PL intensity

26 significantly decreased with increase in the loading amount of $Na_2CoP_2O_7$, indicating that

27 the co-catalyst also improves the charge separation of PCNBA samples (Figure 5B).

28 Photocurrent (I_{ph}) measurements of the samples showed a significant increase in I_{ph} of

29 PCNBA0.2 compared to that of pristine PCN (Figure 5C), indicating enhanced efficiency

30 of the charge separation. With loading of $Na_2CoP_2O_7$, I_{ph} was further enhanced, indicating

1 that the co-catalyst loading also significantly suppressed recombination, leading to an

2 improved charge transference. Moreover, the diameter of semicircle (PCNBA0.2Co5%)

3 was the smallest in Nyquist plots measurements by the A. C. electrochemical impedance

4 spectra (EIS) (Figure 5D), indicating that PCNBA0.2Co5% showed the best charge

5 transfer. Therefore, co-polymerization of BA units and loading of a co-catalyst

6 significantly suppressed charge recombination and promoted charge transfer of the

7 PCNBA, leading to an enhanced photocatalytic H_2O_2 production.

8 **Here is Figure 6.**

9 The possible photo-redox reactions in the PCNBA0.2 system are summarized in

10 Figure 6A. An ORR reaction via the one-electron transfer pathway is a competitive

11 reaction for H_2O_2 generation at the reduction side. Water oxidation via the 4-electron

12 pathway to generate O_2 and water oxidation via the 2-electron pathway to generate H_2O_2

13 are competitive reactions at the oxidation side as follows:

14 $$O_2 + 2e^- + 2H^+ \rightarrow H_2O_2 \ +0.28 \text{ V vs. RHE (pH=7)} \tag{6}$$

15 $$2H_2O - 2e^- \rightarrow H_2O_2 + 2H^+ \ +1.35 \text{ V vs. RHE (pH=7)} \tag{7}$$

16 The CBM and VBM of PCNBA0.2 are -0.58 V and 1.85 V, respectively, indicating that

17 both eq. 6 and eq. 7 are thermodynamically possible [46]. Ag^+ was added into the system

18 as an electron acceptor to improve charge separation, resulting in acceleration of the

19 photocatalytic oxidation reactions. As shown in Figure S16 and Figure S17, O_2 was

20 steadily generated when Ag^+ was added, whereas H_2O_2 was hardly detected in the

21 photocatalytic system of either PCNBA0.2 or PCNBA0.2Co5%. These results proved that

22 H_2O_2 production does not originate from the photocatalytic water oxidation reactions. It

23 should be noted that the activities of PCN samples for photocatalytic oxygen evolution

24 reactions (OERs) were significantly increased after the band engineering and were

25 further increased by the loading of $Na_2CoP_2O_7$. These results revealed that the more

26 positive VBM of PCNBA promotes the OER activity and that $Na_2CoP_2O_7$ behaves as a

27 co-catalyst for water oxidation. The accelerated OER may further increase the overall

28 reaction rate for photocatalytic H_2O_2 production from water and oxygen.

29 Since H_2O_2 can be generated via a one-step, two-electron transfer reaction or via a

30 stepwise one-electron transfer reaction (Figure 6A), rotating disk electrode (RDE)

1 analysis were conducted to investigate the properties of the electron transfer to O_2 on

2 PCN samples. The number of electrons (n) transferred to O_2 were estimated by the

3 results obtained from the slope value of Koutecky–Levich plots (Figure 6B and S18). The

4 estimated "n" value was 1.4 for pristine PCN, indicating that one-electron reduction

5 dominates in the photocatalytic O_2 reduction. In the case of PCNBA0.2Co5%, the

6 estimated "n" value was close to 2, indicating that O_2 molecules were reduced via an

7 apparent two-electron transfer reaction. To get the insight of the intermediate products

8 during photocatalytic H_2O_2 production, sacrificial reagents for quenching of active species

9 quenching were added into the system. As shown in Figure 6C, with the addition of a $\cdot O_2^-$

10 scavenger, p-benzoquinone (BQ. 1 mM), the H_2O_2 production significantly decreased in

11 all PCN photocatalytic systems, indicating that $\cdot O_2^-$ is a crucial intermediate during

12 photocatalytic H_2O_2 production. This result supports the previous theory that the H_2O_2

13 production catalyzed by a PCN-based photocatalyst is a rapid step-wise one-electron to

14 one-electron reaction [12-19], which was first proposed by Prof. Shiraishi and co-workers.

15 The magnitude of decrease in H_2O_2 production with the addition of BQ followed the

16 sequence of PCN, PCNBA0.2 and PCNBA0.2Co5%, indicating less lifetime of $\cdot O_2^-$ in

17 PCNBA0.2 systems [47], i. e., the generated $\cdot O_2^-$ may rapidly be further reduced to form

18 1,4-endoperoxide. In the case of pristine PCN, the generated $\cdot O_2^-$ may hardly be reduced

19 to form 1,4-endoperoxide, resulting in the accumulation of $\cdot O_2^-$.

20 ESR analysis also confirmed the results of scavenger quenching experiments

21 (Figure 6D). When methanol was used as a solvent and electron donor, 6

22 characterization peaks of DMPO-$\cdot O_2^-$ were observed in the spectrum of PCN, indicating

23 that the superoxide radical is an intermediate product during photocatalytic H_2O_2

24 production [37]. The peak intensity of DMPO-$\cdot O_2^-$ in the PCNBA0.2 system slightly

25 decreased, and the intensity significantly decreased in the PCNBA0.2Co5% system. The

26 rapid reduction of $\cdot O_2^-$ in the photocatalytic system of PCNBA0.2Co5% could be

27 attributed to the promoted charge separation. The improved charge separation results in

28 a high density of photoelectrons trapped in the CB, which could accelerate further

29 reduction of $\cdot O_2^-$ to form 1,4-endoperoxide (Scheme 2) [16], rather than to remain as $\cdot O_2^-$

1 in the case of pristine PCN. Therefore, the apparent electron transfer number was

2 calculated to be 2 in the PCNBA0.2Co5% system, which significantly promoted the H_2O_2

3 production.

4 **Here is Scheme 2.**

5   Alkali metal incorporated with a PCN framework has been reported to significantly

6 promote the production of H_2O_2 with the existence of electron donors [11, 12, 14]. As

7 shown in Figure 6E, PCN samples incorporated with alkali metal ions (PCNK10 and

8 PCNNa10) showed almost triple activity improvement compared with the activity of

9 PCNBA0.2Co5% with the addition of ethanol as an electron donor. On the other hand,

10 PCNK10 and PCNNa10 showed no improvement of H_2O_2 production without the addition

11 of sacrificial reagents. The inferior performance of PCNK10 and PCNNa10 may be due to

12 the constant VBM of PCNs incorporated alkali metals ions [12, 49]. The shallow VBM of

13 PCNK10 could not overcome the large potential of water oxidation (>0.8 V). This result

14 revealed the crucial role of band-engineering for improving photocatalytic H_2O_2

15 production using water and oxygen (Scheme 2).

16 **Here. Figure 7.**

17   To elucidate the insight of the band engineering introduced by the BA motif, density

18 function theory calculations combined with analysis of the density of states was

19 conducted by inserting one or two BA units (i. e., Melem_4BA1 and Melem_4BA2) into

20 the melon molecules. A model composed of 4 melem units was also constructed to

21 present melon molecules (Melem_4). Detailed optimization and frequency calculation

22 results are shown in Figure S19-21 Tables S1-3. The calculation results showed that the

23 value of E_g was 7.73 eV. It was larger than the value obtained from the DRS discussed

24 above (2.77 eV), which was due to the limited model size and the known limitation of DFT

25 [49, 50]. In this case, this work discussed the changing tendency of calculated E_g and the

26 band positions based on the experimental results, which could validate the band

27 engineering induced by BA motifs. As shown in Figure 7A, E_g of Melem_4BA2 narrowed

28 after modification with BA motifs compared with E_g of Melem_4. The calculated CBM and

29 VBM of Melem_4BA1 and Melem_4BA2 also showed an obvious positive shift compared

30 with those of Melem_4. The calculated potential of the bandgap width and the shift in

1   band positions showed the same tendency as that in experimental results, indicating that

2   the BA motifs inserted in the melon matrix result in induction of a positive shift of VBMs.

3

4   To further investigate the electronic properties of the PCNBA samples, the total DOS

5   and partial DOS of Melem_4, Melem_4BA1 and Melem_4BA2 were obtained, as shown

6   in Figures 7B-F [51]. For Melem_4, representing pristine PCNs, the partial DOS showed

7   that its valence band (VB) and conduction band (CB) consist of N 2p and C 2p states,

8   respectively. For Melem_4BA1 and Melem_4BA2, their CBs also consist of N 2p and C

9   2p states, whereas O 2p state did not appear in composition states of the CBM. However,

10   the VB of Melem_4BA2 is mainly composed of N 2p, C 2p and O 2p states. Since the

11   electronic potential of O 2p is much more positive than that of N 2p and C 2p, as shown in

12   Figure 7C and 7F, N 2p, C 2p and O 2p states of Melem_4BA1 and Melem_4BA2 formed

13   more positive VBM compared with the VBMs consisting with only N 2p and C 2p states

14   (Melem_4). The partial DOS of molecular fragments also indicates that the inserted BA

15   fragments result in the positive shift of band positions (Figure 7B and 7E). Therefore, we

16   could draw a conclusion that the band engineering induced by BA motifs is due to the O

17   2p states introduced by BA units. The co-polymerization of nitrogen-rich precursors and

18   oxygen-rich motifs has been theoretically proved for the first time to result in a more

19   positive band position, thus providing a new approach for designing efficient

20   photocatalytic systems for nonsacrificial H_2O_2 production.

21

22   **4. Conclusion**

23   In summary, the band positions of polymetric carbon nitride can be rationally

24   designed by using melem and barbituric acid as precursors for efficient photocatalytic

25   H_2O_2 production. The C=O groups incorporated in the PCN matrix formed a positive

26   valence band with sufficient potential (1.85 eV vs. SHE) for overcoming the large

27   overpotential of water oxidation (c.a.>0.8 V). The light absorption edge also expanded

28   from 450 to 550 nm, indicating the promoted light harvesting. With the further loading of

29   $Na_2CoP_2O_7$ as an OER co-catalyst, the PCNBAs showed a record-high apparent

30   quantum yield of 8.0% and a SCC of 0.30% for photocatalytic H_2O_2 production with only

1   H_2O and O_2. The co-polymerization of BA and melem, as well as the loading of

2    $Na_2CoP_2O_7$ significantly improved the charge separation. Analysis by DFT calculation

3   combined with DOS showed that the positive shift of the band position is due to the O 2p

4   states introduced by the co-polymerization of BA units. Co-polymerization of oxygen-rich

5   motifs has been proven for the first time to be an effective approach for developing

6   catalytic systems for enhanced H_2O_2 production in the aspect of electronic energy level.

7   Therefore, this work provides not only a primary guideline for designing an appropriate

8   band structure but also a practical approach to achieve the optimized performance for

9   photocatalytic H_2O_2 production with a PCN-based material.

10

22

23   **Author Contribution:**

24   **Zhenyuan Teng:** Conceptualization, Methodology, Computations and Writing-Original

25   draft preparation. **Wenan Cai**: Material preparation, measurements of photocatalytic

26   activity, photoelectrochemical measurements. **Sixiao Liu**: Material characterization,

27   Investigation, Software. *Chengyin Wang:* Supervision, Reviewing and Editing. *Qitao*

28   *Zhang*: Conceptualization, Supervision, Software, Reviewing and Editing. **Chenliang Su**:

29   Writing-Reviewing and Editing. *Teruhisa Ohno:* Conceptualization, Supervision,

1   Reviewing and Editing.

2

3   **Declaration of Interests**

4   The authors declare no competing financial interest.

5

6   References

7   [1]   K.P. Bryliakov, Catalytic asymmetric oxygenations with the environmentally benign

8   oxidants H_2O_2 and O_2, Chem. Rev. 117 (2017) 11406-11459.

9   https://doi.org/10.1021/acs.chemrev.7b00167.

10   [2]   M. Nakano, I. Uchiyama, H. Takamatsu, Method for cleaning semiconductor wafers,

11   US Patent (1995) US5626681A.

12   [3]   T. Kitano, Etching solution and etching method for semiconductors, US Patent (1993)

13   US5419808A.

14   [4]   E. Neyens, J. Baeyens, A review of classic Fenton's peroxidation as an advanced

15   oxidation technique, J. Hazard. Mater. 98 (2003) 33-50.

16   https://doi.org/10.1016/S0304-3894(02)00282-0.

17   [5]   S.A.M. Shaegh, N.-T. Nguyen, S.M.M. Ehteshamiab, S.H. Chan, A membraneless

18   hydrogen peroxidefuel cell using Prussian Blue as cathode material, Energy Environ.

19   Sci. 5 (2012) 8225-8228. https://doi.org/10.1039/C2EE21806B.

20   [6]   F. Sandelin, P. Oinas, T. Salmi, J. Paloniemi, H. Haario, Kinetics of the recovery of

21   active anthraquinones, Ind. Eng.Chem. Res. 45 (2006) 986-992.

22   https://doi.org/10.1021/ie050593s.

23   [7]   J.K. Edwards, B.E. Solsona, P. Landon, A.F. Carley, A. Herzing, C.J. Kiely, G.J.

24   Hutchings, Direct synthesis of hydrogen peroxide from H_2 and O_2 using

25   TiO_2-supported Au–Pd catalysts, J. Catal. 236 (2005) 69-79.

26   https://doi.org/10.1016/j.jcat.2005.09.015.

27   [8]   J.C. Pritchard, Q. He, E.N. Ntainjua, M. Piccinini, J.K. Edwards, A.A. Herzing, A.F.

28   Carley, J.A. Moulijn, C.J. Kiely, G.J. Hutchings, The effect of catalystpreparation

29   method on the performance of supported Au–Pd catalysts for the direct synthesis of

30   hydrogen peroxide, Green Chem. 12 (2010) 915-921.

31   https://doi.org/10.1039/B924472G.

32   [9]   K. Fuku, K. Sayama, Efficient oxidative hydrogen peroxide production and

33   accumulation in photoelectrochemical water splitting using a tungsten

34   trioxide/bismuth vanadate photoanode, Chem. Commun. 52 (2016) 5406-5409.

35   https://doi.org/10.1039/C6CC01605G.

36   [10] K. Fuku,   Y. Miyase,   Y. Miseki, T. Funaki, T. Gunji, K. Sayama,

37   Photoelectrochemical hydrogen peroxide production from water on a $WO_3/BiVO_4$

38   photoanode and from O_2 on an au cathode without external bias, Chem. Asian J. 12

39   (2017) 1111-1119. https://doi.org/10.1002/asia.201700292.

40   [11] P. Zhang, D. Sun, A. Cho, S. Weon, S. Lee, J. Lee, J. W. Han, D.-P. Kim, W. Choi,

41   Modified carbon nitride nanozyme as bifunctional glucose oxidase-peroxidase for

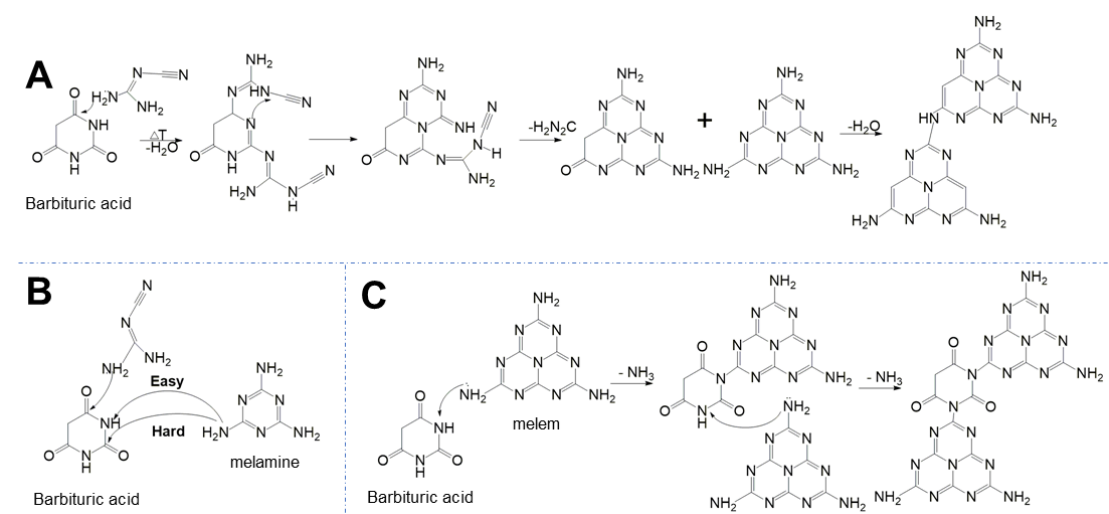42   metal-free bioinspired cascade photocatalysis, Nat. Comm. (2019). https://doi.org/

43   10.1038/s41467-019-08731-y.

[12] G. Moon, M. Fujitsuka, S. Kim, T. Majima, X. Wang, W. Choi, Photochemical production of H_2O_2 through O_2 reduction over carbon nitride frameworks incorporated with multiple heteroelements, ACS Catal. 7 (2017) 2886-2895. https://doi.org/10.1021/acscatal.6b03334.

[13] S. Kim, G. Moon, H. Kim, Y. Mun, P. Zhang, J. Lee, W. Choi, Selective charge transfer to dioxygen on KPF_6-modified carbon nitride for photocatalytic synthesis of H_2O_2 under visible light, J. Catal. 357 (2018) 51-58. https://doi.org/10.1016/j.jcat.2017.10.002.

[14] H. Kim, Y. Choi, S. Hu, W. Choi, J.-H. Kim, Photocatalytic hydrogen peroxide production by anthraquinone-augmented polymeric carbon nitride, APPL CATAL B-ENVIRON. 229, (2018) 121-129. https://doi.org/10.1016/j.apcatb.2018.01.060.

[15] Y. Kofuji, Y. Isobe, Y. Shiraishi, H. Sakamoto, S. Tanaka, S. Ichikawa, T. Hirai, Carbon nitride–aromatic diimide–graphene nanohybrids: Metal-free photocatalysts for solar-to-hydrogen peroxide energy conversion with 0.2% efficiency, J. Am. Chem. Soc. 138 (2016) 10019-10025. https://doi.org/10.1021/jacs.6b05806.

[16] Y. Shiraishi, S. Kanazawa, Y. Kofuji, H. Sakamoto, S. Ichikawa, S. Tanaka, T. Hirai, Sunlight-driven hydrogen peroxide production from water and molecular oxygen by metal-free photocatalysts, Angew. Chem. 126 (2014) 13672 -13677. https://doi.org/10.1002/anie.201407938.

[17] Y. Kofuji, S. Ohkita, Y. Shiraishi, H. Sakamoto, S. Tanaka, S. Ichikawa, T. Hirai, Graphitic carbon nitride doped with biphenyl diimide: Efficient photocatalyst for hydrogen peroxide production from water and molecular oxygen by sunlight, ACS Catal. 6 (2016) 7021-7029. https://doi.org/10.1021/acscatal.6b02367.

[18] Y. Shiraishi, T. Takii, T. Hagi, S. Mori, Y. Kofuji, Y. Kitagawa, S. Tanaka, S. Ichikawa, T. Hirai, Resorcinol–formaldehyde resins as metal-free semiconductor photocatalysts for solar-to-hydrogen peroxide energy conversion, Nat. Mater. 18, (2019) 985-993. https://doi.org/10.1038/s41563-019-0398-0.

[19] Z. Wei, M. Liu, Z. Zhang, W. Yao, H. Tanban, Y. Zhu, Efficient visible-light-driven selective oxygen reduction to hydrogen peroxide by oxygen-enriched graphitic carbon nitride polymer, Energy Environ. Sci. 11 (2018) 2581-2589. https://doi.org/10.1039/C8EE01316K.

[20] M. Teranishi, S. Naya, H. Tada, Temperature- and pH-dependence of hydrogen peroxide formation from molecular oxygen by gold nanoparticle-loaded titanium(IV) oxide photocatalyst, J. Phys. Chem. C 120 (2016) 1083-1088. https://doi.org/10.1021/acs.jpcc.5b10626.

[21] D. Tsukamoto, A. Shiro, Y. Shiraishi, Y. Sugano, S. Ichikawa, S. Tanaka, T. Hirai, Photocatalytic H_2O_2 production from ethanol/O_2 system using TiO_2 loaded with Au–Ag bimetallic alloy nanoparticles, ACS Catal. 2 (2012) 599-603. https://doi.org/10.1021/cs2006873.

[22] Y. Shiraishi, S. Kanazawa, D. Tsukamoto, A. Shiro, Y. Sugano, T. Hirai, Selective hydrogen peroxide formation by titanium dioxide photocatalysis with benzylic alcohols and molecular oxygen in water, ACS Catal. 3 (2013) 2222−2227. https://doi.org/10.1021/cs400511q.

[23] N. Kaynan, B.A. Berke, O. Hazut, R. Yerushalmi, Sustainable photocatalytic production of hydrogen peroxide from water and molecular oxygen, J. Mater. Chem. A 2 (2014) 13822−13826. https://doi.org/10.1039/c4ta03004d.

[24] G.-H. Moon, W. Kim, A.D. Bokare, N.-E. Sung, W. Choi, Solar production of H_2O_2 on reduced graphene oxide-TiO_2 hybrid photocatalysts consisting of earth-abundant elements only, Energy Environ. Sci. 7 (2014) 4023−4028. https://doi.org/10.1039/C4EE02757D.

[25] H.-I. Kim, O. S. Kwon, S. Kim, W. Choi, J.-H. Kim, Solar production of H_2O_2 on reduced graphene oxide-TiO_2 hybrid photocatalysts consisting of earth-abundant elements only, Energy Environ. Sci. 9 (2016) 1063-1073. https://doi.org/10.1039/C4EE02757D.

[26] X. Wang, K. Maeda, A. Thomas, K. Takanabe, G. Xin, J. M. Carlsson, K. Domen, M. Antonietti, A metal-free polymeric photocatalyst for hydrogen production from water under visible light, Nat. Mater. 8 (2009) 76−80. https://doi.org/10.1038/nmat2317.

[27] J. Zhang, X. Chen, K. Takanabe, K. Maeda, K. Domen, J. D. Epping, X. Fu, M. Antonietti, X. Wang, Synthesis of a carbon nitride structure for visible-light catalysis by copolymerization, Angew. Chem. Int. Ed. 49 (2010) 441-444. https://doi.org/10.1002/anie.200903886.

[28] J. Zhang, G. Zhang, X. Chen, S. Lin, L. Möhlmann, G. Doł̦ega, G. Lipner, M. Antonietti, S. Blechert, X. Wang, Co-monomer control of carbon nitride semiconductors to optimize hydrogen evolution with visible light, Angew. Chem. Int. Ed. 51 (2012) 3183-3187. https://doi.org/10.1002/anie.201106656.

[29] J. Zhang, M. Zhang, R.Q. Sun, X. Wang, A facile band alignment of polymeric carbon nitride semiconductors to construct isotype heterojunctions, Angew. Chem. 124 (2012) 10292-10296. https://doi.org/10.1002/anie.201205333.

[30] M. Zhang, X. Wang, Two dimensional conjugated polymers with enhanced optical absorption and charge separation for photocatalytic hydrogen evolution, Ener. Environ. Sci. 7 (2014) 1902-1906. https://doi.org/10.1039/C3EE44189J.

[31] J. Qin, S. Wang, H. Ren, Y. Hou, X. Wang, Photocatalytic reduction of CO_2 by graphitic carbon nitride polymers derived from urea and barbituric acid, APPL CATAL B-ENVIRON. 179 (2015) 1-8. https://doi.org/10.1016/j.apcatb.2015.05.005.

[32] B. Jürgens, E. Irran, J. Senker, P. Kroll, H. Müller, W. Schnick, Melem (2,5,8-triamino-tri-s-triazine), an important intermediate during condensation of melamine rings to graphitic carbon nitride: Synthesis, structure determination by X-ray powder diffractometry, solid-state NMR, and theoretical studies, J. Am. Chem. Soc. 125 (2003) 10288-10300. https://doi.org/10.1021/ja0357689.

[33] H. Kim, J. Park, I. Park, K. Jin, S. E. Jerng, S. H. Kim, K. T. Nam, K. Kang, Coordination tuning of cobalt phosphates towards efficient water oxidation catalyst, Nat. Commun 6 (2015) 8253. https://doi.org/10.1038/ncomms9253.

[34] F. Erragh, A. Boukhari, B. Elouadi, E. M. Holt, Disodium zinc pyrophosphate and disodium (europium) zinc pyrophosphate, J. Crystallogr. Spectrosc. Res. 21 (1991) 321-326. https://doi.org/10.1107/S0108270198006246.

[35] Z. Teng, H. Lv, C. Wang, H. Xue, H. Pang, G. Wang, Bandgap engineering of ultrathin graphene-like carbon nitride nanosheets with controllable oxygenous

functionalization, CARBON 113 (2017) 63-75.
https://doi.org/10.1016/j.carbon.2016.11.030.

[36] J.D. Figueroa-Villar, S.C.G. de Oliveira, Synthesis and mechanism of formation of oxadeazaflavines by microwave thermal cyclization of ortho-halobenzylidene barbiturates, J. Braz. Chem. Soc. 22 (2011) 2101-2107. http://dx.doi.org/10.1590/S0103-50532011001100012.

[37] Z. Teng, N. Yang, H. Lv, S. Wang, Ma. Hu, C. Wang, D. Wang, G. Wang, Edge-functionalized g-C_3N_4 nanosheets as a highly efficient metal-free photocatalyst for safe drinking water, Chem 5 (2019) 664–680. https://doi.org/10.1016/j.chempr.2018.12.009.

[38] H. Hirakawa, M. Hashimoto, Y. Shiraishi, T. Hirai, Photocatalytic conversion of nitrogen to ammonia with water on surface oxygen vacancies of titanium dioxide, J. Am. Chem. Soc., 139 (2017) 10929-10936. https://doi.org/10.1021/jacs.7b06634.

[39] H. Sakamoto, T. Ohara, N. Yasumoto, Y. Shiraishi, S. Ichikawa, S. Tanaka, T. Hirai, Hot-electron-induced highly efficient O_2 activation by Pt nanoparticles supported on Ta_2O_5 driven by visible light, J. Am. Chem. Soc., 137 (2015) 9324-9332. https://doi.org/10.1021/jacs.5b04062.

[40] H. Wang, T. Lindgren, J. He, A. Hagfeldt, S.-E. Lindquist, Photolelectrochemistry of nanostructured WO_3 thin film electrodes for water oxidation: Mechanism of electron transport, J. Phys. Chem. B 104 (2000) 5686-5696. https://doi.org/10.1021/jp0002751.

[41] Q. Mi, Y. Ping, Y. Li, B. Cao, B.S. Brunschwig, P.G. Khalifah, G.A. Galli, H.B. Gray, N.S. Lewis, Thermally stable N_2-intercalated WO_3 photoanodes for water oxidation, J. Am. Chem. Soc. 134 (2012) 18318-18324. https://doi.org/10.1021/ja3067622.

[42] T.W. Kim, K.-S. Choi, Nanoporous $BiVO_4$ photoanodes with dual-layer oxygen evolution catalysts for solar water splitting, Science 343 (2014) 990-994. https://doi.org/10.1126/science.1246913.

[43] H. Kim, S. Lee, Y.-U. Park, H. Kim, J. Kim, S. Jeon, K. Kang, Neutron and X-ray diffraction study of pyrophosphate-based $Li_{2-x}MP_2O_7$ (M = Fe, Co) for lithium rechargeable battery electrodes, Chem. Mater. 23 (2011) 3930-3937. https://doi.org/10.1021/cm201305z.

[44] Q. Wang, K. Domen, Particulate photocatalysts for light-driven water splitting: Mechanisms, challenges, and design strategies, Chem. Rev. (2019) https://doi.org/10.1021/acs.chemrev.9b00201.

[45] Y. Kofuji, Y. Isobe, Y. Shiraishi, H. Sakamoto, S. Ichikawa, S. Tanaka, T. Hirai, Hydrogen peroxide production on a carbon nitride-boron nitride-reduced graphene oxide hybrid photocatalyst under visible light, 10 (2018) 2070-2077. https://doi.org/10.1002/cctc.201701683.

[46] L. Chen, L. Wang, Y. Wan, Y. Zhang, Z. Qi, X. Wu, H. Xu, Acetylene and diacetylene functionalized covalent triazine frameworks as metal-free photocatalysts for hydrogen peroxide production: A new two-electron water oxidation pathway, Adv. Mater. 2019, (2019) 1904433. https://doi.org/10.1002/adma.201904433.

[47] Y. Peng, L. Wang, Y. Liu, H. Chen, J. Lei, J. Zhang, Visible-light-driven photocatalytic H_2O_2 production on g-C_3N_4 loaded with CoP as a noble metal free cocatalyst, Eur. J. Inorg. Chem. 2017 (2017), 4797-4802. https://doi.org/10.1002/ejic.201700930.

[48] C. Qiu, Y. Xu, X. Fan, D. Xu, R. Tandiana, X. Ling, Y. Jiang, C. Liu, L. Yu, W. Chen, C. Su, Highly crystalline K-intercalated polymeric carbon nitride for visible-light photocatalytic alkenes and alkynes deuterations, Adv. Sci. 6 (2018) 1801403. https://doi.org/10.1002/advs.201801403.

[49] K. Wang, Q. Li, B. Liu, B. Cheng, W. Ho, J. Yu, Sulfur-doped g-C_3N_4 with enhanced photocatalytic CO_2-reduction performance, APPL CATAL B-ENVIRON. 176-177 (2015) 44-52. https://doi.org/10.1016/j.apcatb.2015.03.045.

[50] X.W. Li, J. Zhou, Q. Wang, Y. Kawazoe, P. Jena, Patterning graphitic C–N sheets into a kagome lattice for magnetic materials, J. Phys. Chem. Lett. 4 (2013) 259. https://doi.org/10.1021/jz3018804.

[51] T. Lu, F. Chen, Multiwfn: A multifunctional wavefunction analyzer, J. Comput. Chem., 33 (2012) 580-592. https://doi.org/10.1002/jcc.22885.
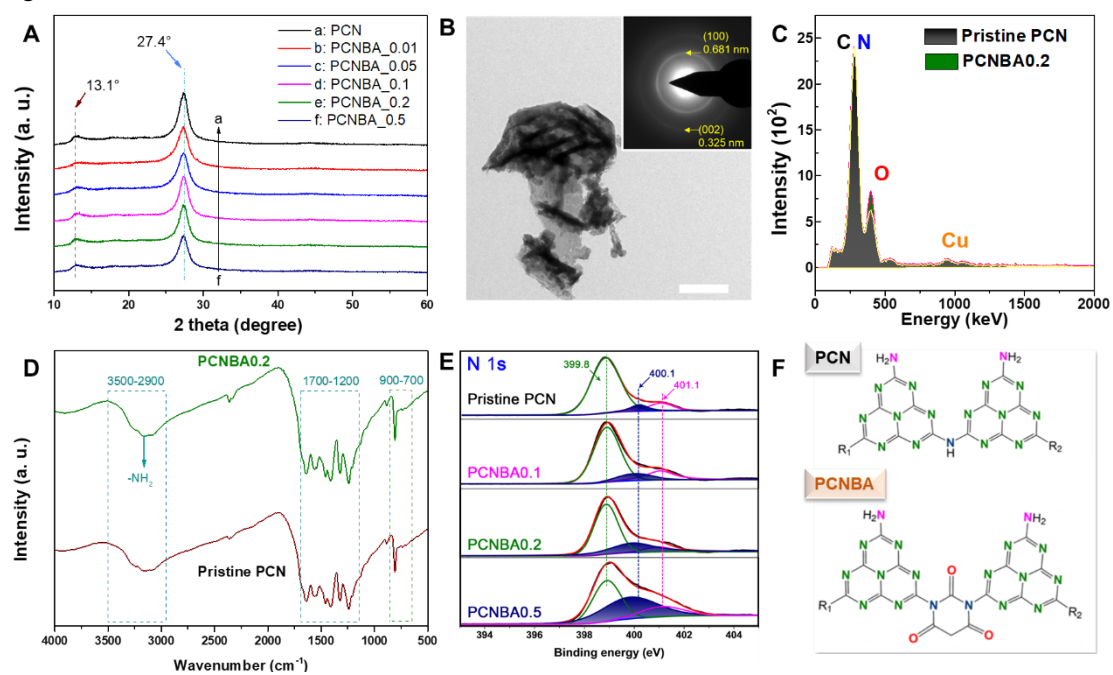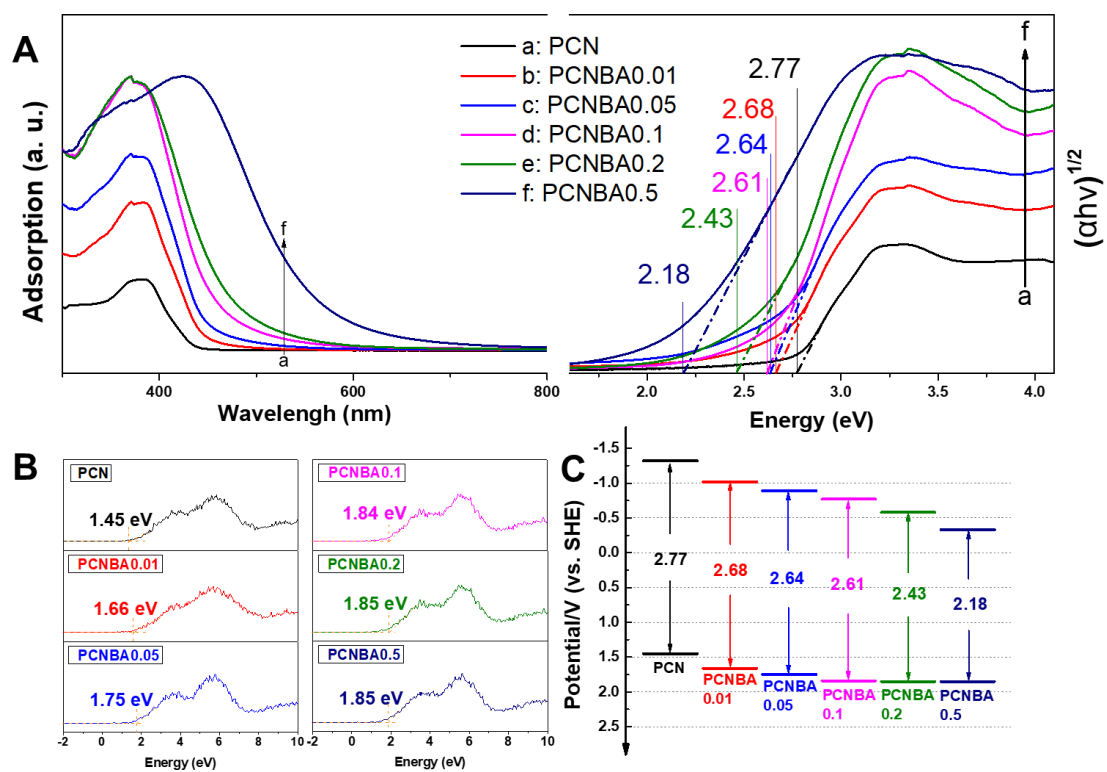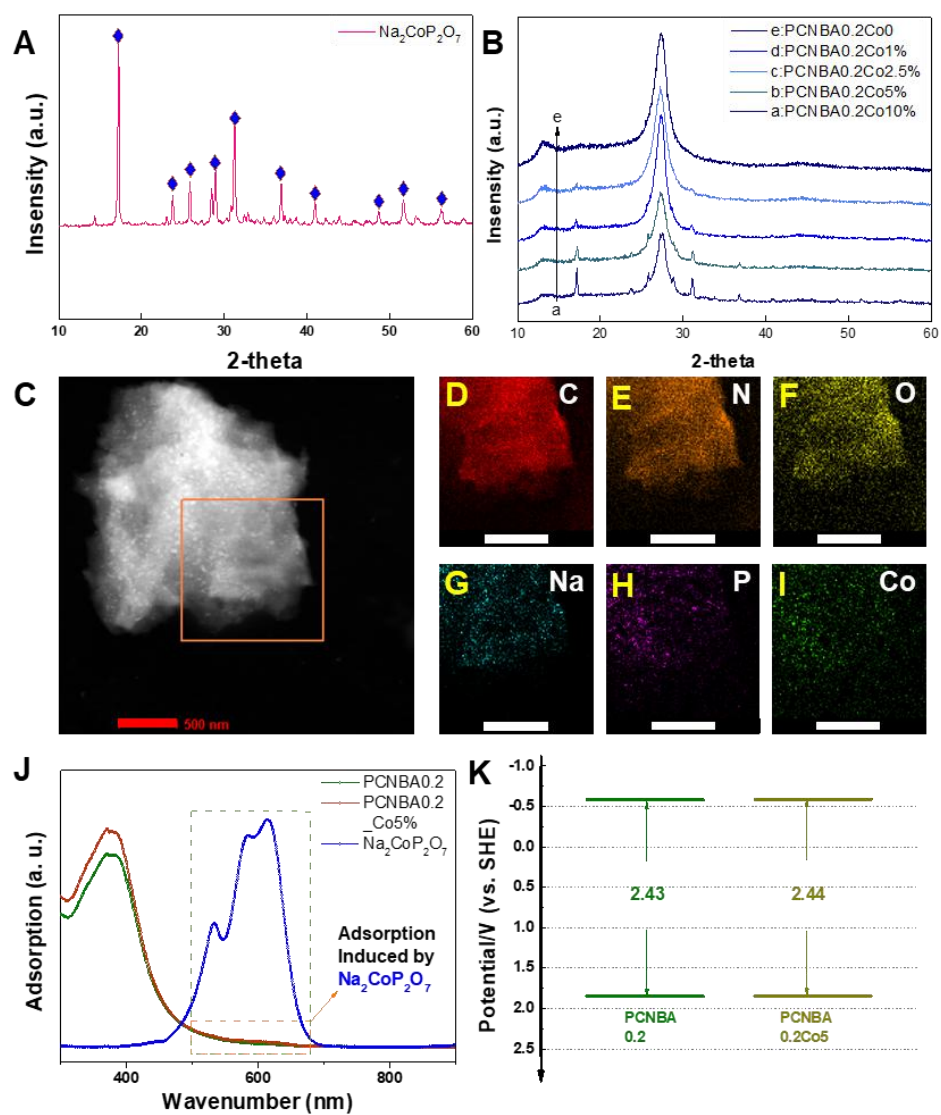
Figure

Scheme 1:

Scheme 2:

Figure 1:

Figure 2:

Figure 3:

Figure 4:

Figure 5:

Figure 6:

A

$O_2 + e^- + H^+ = HO_2 \ (aq)$ $E_{ox/red} = -0.46 \ V$

$2e^- + 2H^+ = H_2$ $E_{ox/red} = -0.41 \ V$

$O_2 + e^- = O_2^-$ $E_{ox/red} = -0.28 \ V$

$O_2 + 2e^- + 2H^+ = H_2O_2$ $E_{ox/red} = 0.28 \ V$

$2H_2O = O_2 + 4e^- + 4H^+$ $E_{ox/red} = 0.82 \ V$

$H_2O_2 + 2e^- + 2H^+ = 2H_2O$ $E_{ox/red} = 1.35 \ V$

CBM = -0.58

VBM = 1.85

$2e^-$

$4h^+$

hv

e^-

h^+

Redox Potential vs NHE (pH=7)

B

Pristine PCN
PCNBA0.2Co5%

n=1.97

n=1.40

$j^{-1} / m^2 A^{-1}$

$\omega^{-1/2} / (rad/s)^{-1/2}$

C

with BQ 57%

with BQ 35%

with BQ 11%

H_2O_2 production surplus (%)

PCNBA0.2 Co5%   PCNBA0.2   PCN

D

PCN
PCNBA0.2
PCNBA0.2Co5

Intensity (10^3 cps)

Magnitic (G)

E

no et-OH

no et-OH

no et-OH

no et-OH

H_2O_2 concentration

PCN BA0.2Co5   PCNBA0.2   PCNK10   PCNNa10
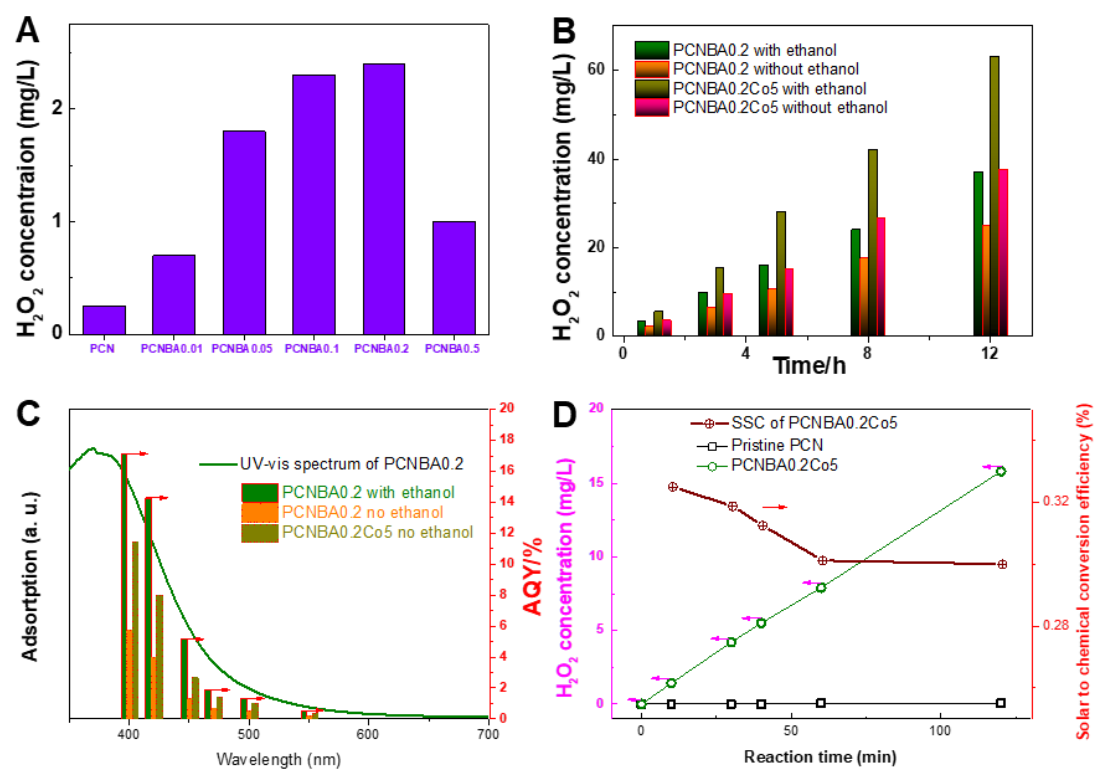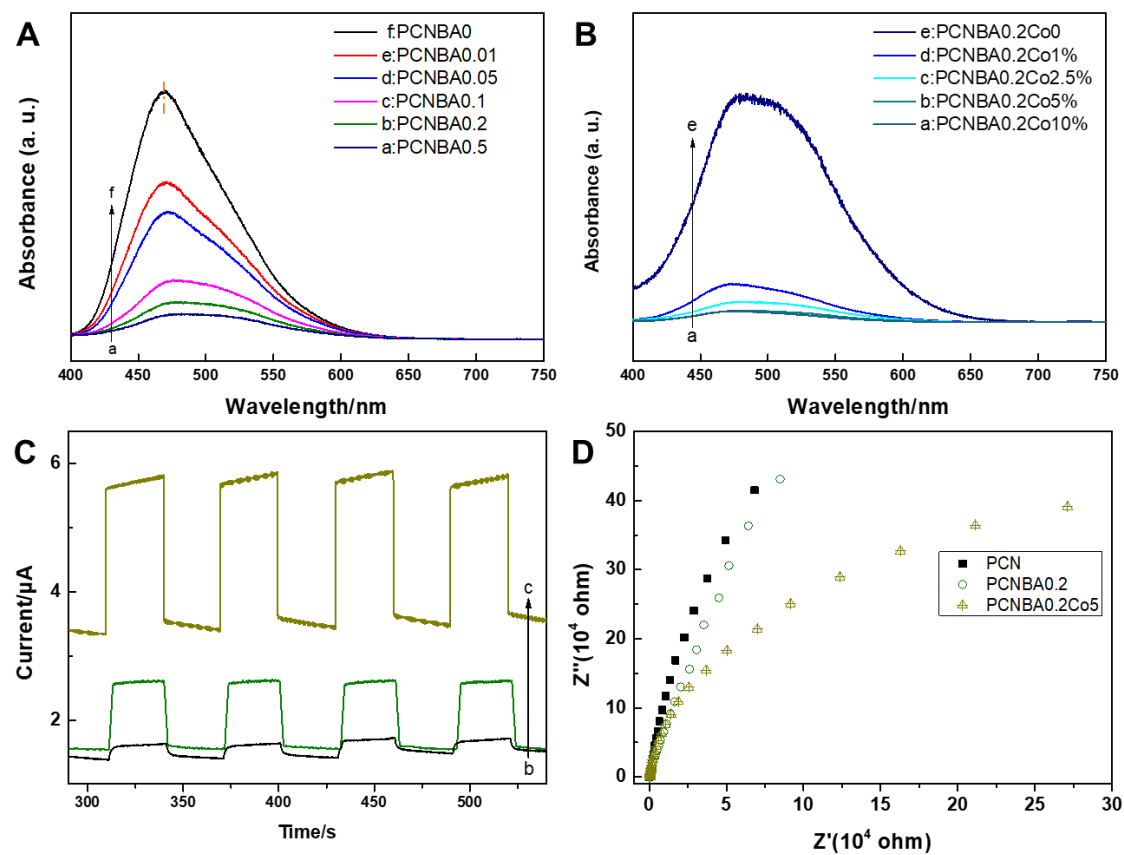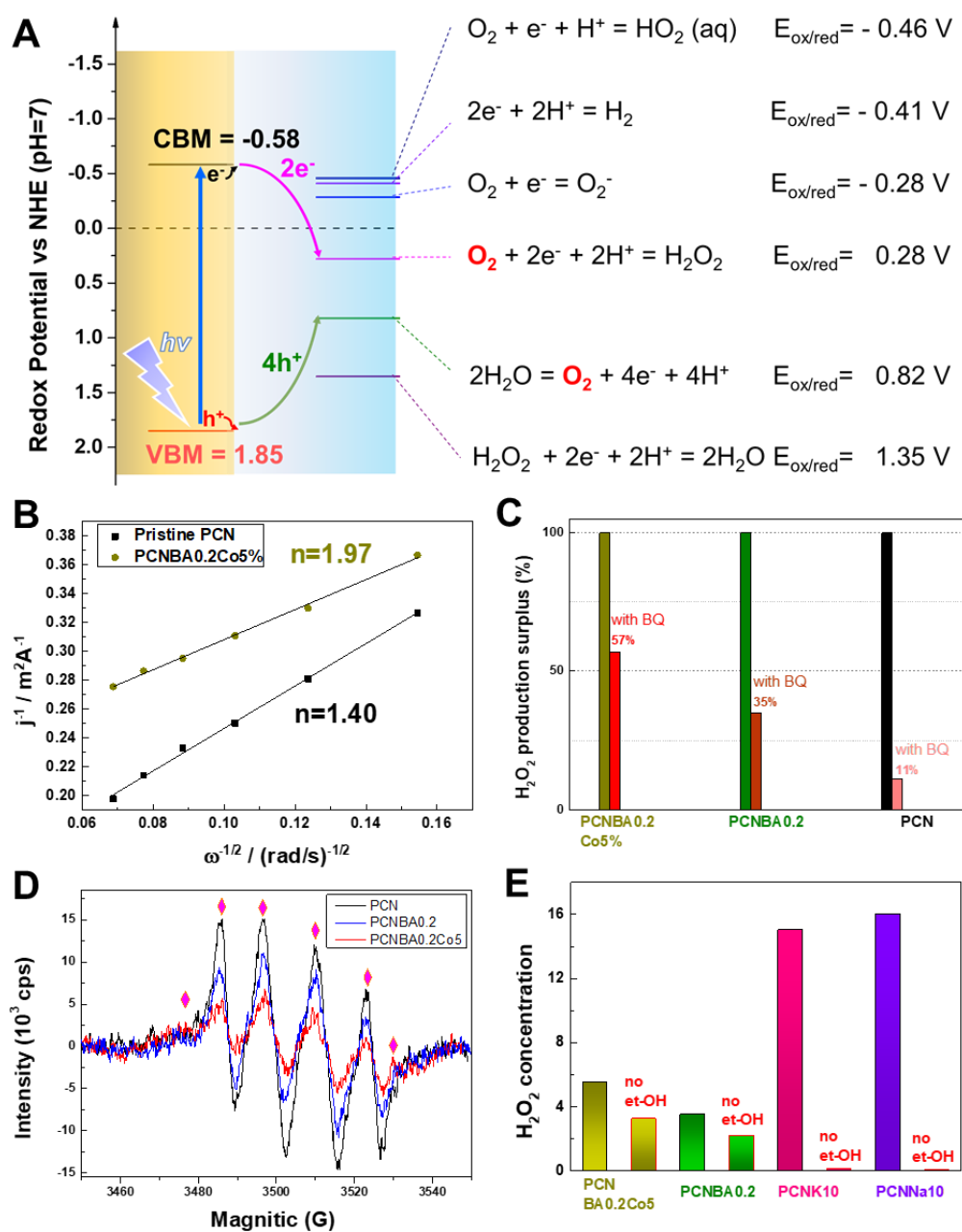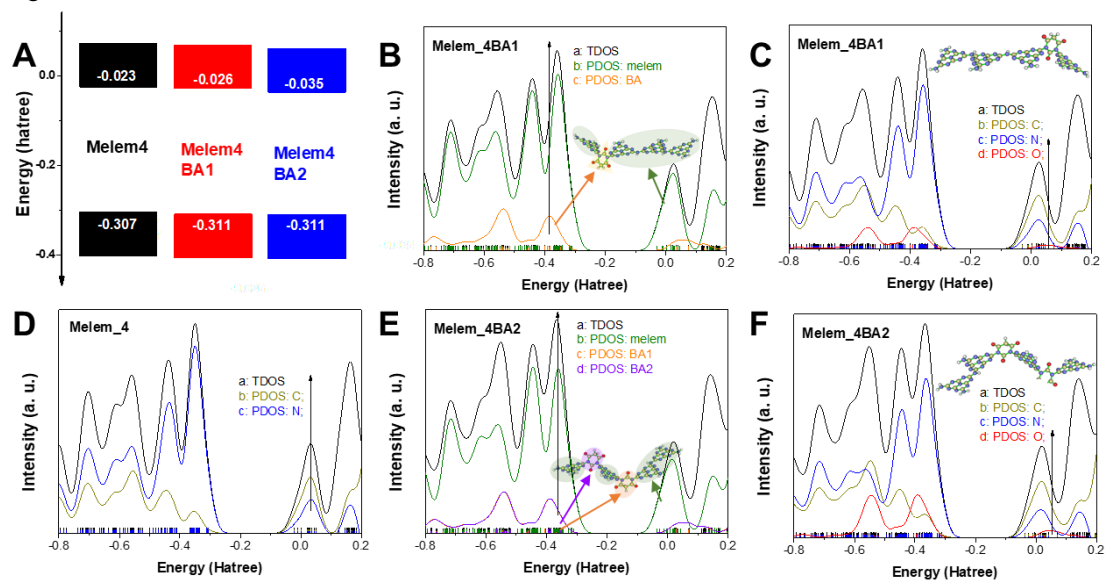
Figure 7:

Captions:

Scheme 1. Thermal polymerization of different nitrogen rich precursors with barbituric acid. Precursors with (A) small molecular weights and (B) large molecular weights. (C) Polymerization process with barbituric acid and melem as precursors.

Scheme 2. Possible reaction route of oxygen evolution reactions using (**A**) pristine PCN or (**B**) PCNBA0.2Co5% as photocatalysts.

Figure 1. Characterization of PCN and PCNBA samples. (A) XRD patterns of pristine PCN and PCNBA samples. (B) TEM image of a PCNBA0.2 sample. The length of scare bar is 1 μm Inserted figure is the SAED pattern of PCNBA0.2. (C) EDX measurements of PCNBA samples. (D) FT-IR spectra of PCN and PCNBA0.2. (E) High-resolution XPS spectra (N1s) with different motif concentrations of PCNs. (F) Possible structure of PCNBA prepared by co-polymerization of melem and barbituric acid.

Figure 2. Band positions of PCN and PCNBAO samples. (**A**) UV-vis spectra of PCN and PCNBAO samples: absorbance spectra on the left and Tauc-plots on the right. (**B**) Valence band XPS of PCN and PCNBA samples. (**C**) Band diagrams of PCN and as-prepared PCNBA samples.

Figure 3. Characterization of co-catalyst-loaded PCNBA. (**A**) XRD patterns of $Na_2CoP_2O_7$. (**B**) XRD patterns of PCNBA loaded with $Na_2CoP_2O_7$ (PCNBAO0.2Co5%). (**C**) HAADF of PCNBA0.2Co5%. STEM EDS mapping images of (**D**) Carbon, (**E**) Nitrogen, (**F**) Oxygen, (**G**) Sodium, (**H**) Phosphorus and (**I**) Cobalt. (**J**) UV-vis absorbance spectra of pure $Na_2CoP_2O_7$ and PCNBAO0.2Co5%. (**K**) Band diagrams of $Na_2CoP_2O_7$ and PCNBAO0.2Co5%.

Figure 4. (A) Results for photocatalytic H_2O_2 production on PCNBAs. Reaction conditions: water (30 mL), catalyst (50 mg), O_2 (1 atm), λ > 420 nm (Xe lamp, light intensity at 400−500 nm: 30.3 W m^{-2}), time (1 h) [15]. (B) Time-dependent change in the amounts of H_2O_2. (C) Absorption spectrum of PCNBA0.2 and action spectra for H_2O_2 formation on the respective catalysts. (D) Time-dependent change in the amounts of H_2O_2 formed and the SCC efficiencies determined under simulated AM1.5G sunlight irradiation.

Figure 5. Photochemical properties of PCNBAs and PCNBA0.2Co5%. Photoluminescence spectra of (**A**) PCN and PCNBA samples and (**B**) PCNBA0.2Co5% under 365 nm excitation. (**C**) Photocurrents of electrodes prepared by PCN, PCNBA0.2 and PCNBA0.5 (line a: pristine PCN; line b: PCNBA0.2; line c: PCNBA0.2Co0.5%). (**D**) EIS of electrodes prepared by PCN, PCNBA0.2 and PCNBA0.5 illuminated under visible light irradiation.

Figure 6. Mechanism of PCNBA0.2 with co-catalyst loading. (A) Possible photo-redox reactions during photocatalytic H_2O_2 production with PCNBA0.2. (B) H_2O_2 production with or without 1 mM BQ in the systems of PCN, PCNBA0.2 and PCNBA0.2Co5%. (C) ESR

spectra of PCN, PCNBA0.2 and PCNBA0.2Co5% in methanol solution using 5,5-diemthyl-1-pyrroline N-oxide as a radical trapper. (D) Koutecky−Levich plots of data obtained by RDE measurements in a buffered pH 7 solution with O_2 at −0.6 V (vs Ag/AgCl). (E) Comparison of the activities of PCNBAs and alkali metal-incorporated PCNs for H_2O_2 production.

Figure 7. Computer simulation of density of states (DOS) with different co-polymerizations of BA motifs. (**A**) Calculated HOMO and LUMO of Melem_4 model (representing PCN), Melem_4BA1 (representing PCNBA with a low motif concentration) and Melem_4BA2 (representing PCNBA with a high motif concentration). Partial DOS and total DOS of the simulated Melem_4 (**D**), Melem_4BA1 (**B**, **E**) and Melem_4BA2 (**C**, **F**). The detailed identification of fragments is shown in Supporting Information.
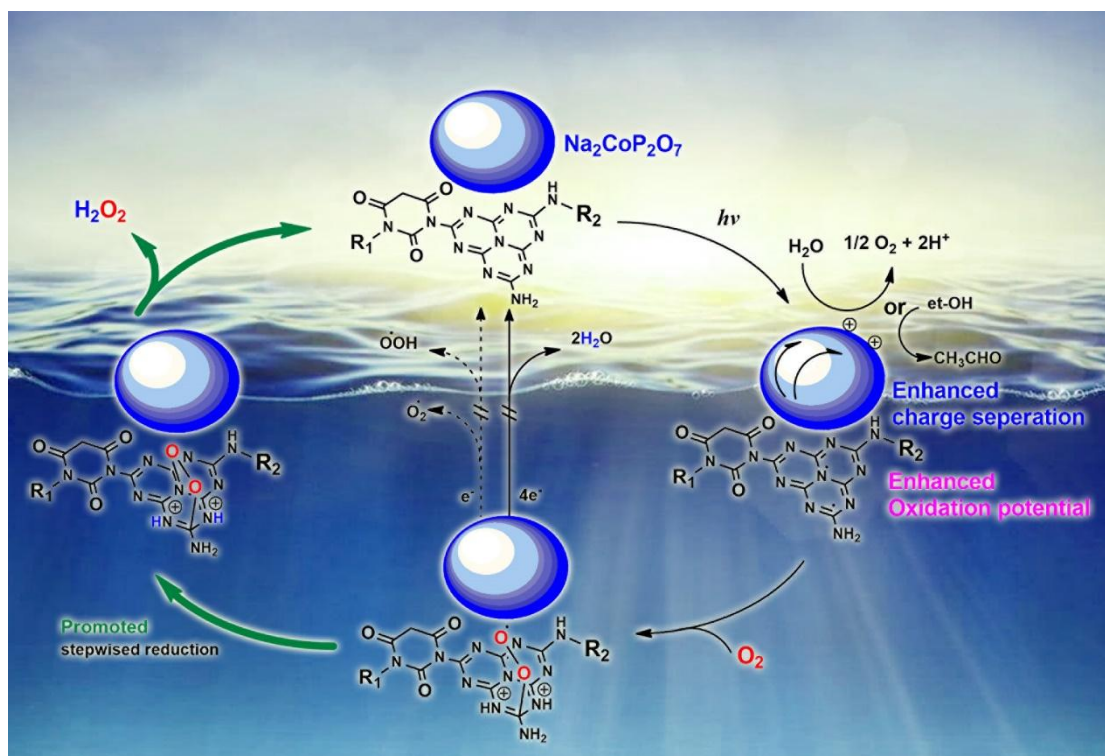
Graphical abstract

Highlights:

1. Polymetric carbon nitrides were prepared by calcinating melem and barbituric acid.
2. As-prepared carbon nitride introduced the C=O in the polymetric matrix.
3. The introduced O 2p states lead to an improved water oxidation ability.
4. The adsorption edge of as-prepared catalyst expanded to 550 nm.
5. The solar to chemical conversion efficiency reached 0.3% for H_2O_2 production.